THE GEOLOGICAL SOCIETY OF AMERICA®

Hydrothermal formation of heavy rare earth element (HREE)–xenotime deposits at 100 °C in a sedimentary basin

Lisa Richter[1,2]*, Larryn W. Diamond[2], Petya Atanasova[3], David A. Banks[4], and Jens Gutzmer[1,3]
[1]Department of Mineralogy, Technical University Bergakademie Freiberg, Freiberg D-09596, Germany
[2]Institute of Geological Sciences, Water-Rock Interaction, University of Bern, Bern CH-3012, Switzerland
[3]Hemholtz Zentrum Dresden-Rossendorf, Helmholtz Institute Freiberg for Resource Technology, Freiberg D-09599, Germany
[4]School of Earth and Environment, University of Leeds, Leeds LS2 9JT, UK

ABSTRACT

Most rare earth element deposits form from magmatic fluids, but there have also been discoveries of heavy rare earth element (HREE)–enriched hydrothermal xenotime deposits within sedimentary basins. As xenotime is notoriously insoluble, the question arises as to whether these lesser-known deposits form at typical basin temperatures or by influx of much hotter magmatic-hydrothermal fluids. The Browns Range District in northern Western Australia hosts deposits of xenotime that are enriched in HREEs and also uranium. The ore bodies consist of fault-controlled hydrothermal quartz-xenotime breccias that crosscut Archean basement rocks and overlying Paleoproterozoic sandstones. Analyses of fluid inclusions show that the xenotime precipitated at remarkably low temperatures, between 100 and 120 °C, in response to decompression boiling. The inclusions contain high excess concentrations of yttrium (10^{-3} mol/kg), REEs ($1–7 \times 10^{-5}$ mol/kg), and uranium (4×10^{-5} mol/kg) in equilibrium with xenotime at these low temperatures, showing that availability of phosphate limited the amount of xenotime precipitated. The analyses further identify SO_4^{2-} and Cl^- as the ligands that facilitated the elevated REE and uranium solubilities. These findings establish that significant REE transport and deposition is feasible at basin temperatures, and hence they raise the potential of unconformity settings for REE exploration. Moreover, the aqueous metal contents support a genetic link between this type of ore fluid and world-class Proterozoic unconformity-related uranium deposits elsewhere.

INTRODUCTION

The vast majority of rare earth element (REE) deposits are known to form at high temperatures in association with carbonatitic and peralkaline magmatism (e.g., Migdisov et al., 2016). However, lesser-known hydrothermal deposits of heavy REE (HREE)–enriched xenotime (YPO_4) also occur within sedimentary basins (e.g., Rabiei et al., 2017). Given the low aqueous solubility of xenotime, it has been unclear if REEs are in fact transported in large quantities at basinal temperatures or if high-temperature magmatic-hydrothermal fluids are required to explain the deposits. Here we address this question by analyzing fluid inclusions in the late Paleoproterozoic Wolverine HREE deposit in the Browns Range of northern Western Australia. Our study yields an unequivocal precipitation temperature for xenotime in the sedimentary environment and defines the solubility, transporting ligands, and precipitation mechanism of yttrium and REEs. It also shows how the ore-bearing fluids may be related to those that form world-class unconformity-related uranium deposits.

GEOLOGICAL SETTING

Located on the northeastern boundary of Western Australia (Fig. 1), the Browns Range HREE district comprises a cluster of fault-hosted, steeply dipping breccia bodies and veins that crosscut the late Archean Browns Range Metamorphics and the unconformably overlying clastic sediments of the Paleoproterozoic Birrindudu Group (Dunster and Ahmad, 2013). At the Wolverine deposit, where the wall rocks are porous arkoses/arenites and conglomerates, the hydrothermal xenotime has been dated to 1646 ± 5 Ma (ion microprobe U-Pb method; Morin-Ka et al., 2016). Thus, the xenotime is much younger than its host rocks, but it is coeval with the Limbunya Group sediments further upsection, which were deposited during active regional faulting (Dunster and Ahmad, 2013). Occurrences of xenotime with similar ages are known within a 200 km radius of Wolverine, most notably at the John Galt (1619 ± 9 Ma; Morin-Ka et al., 2016) and Killi Killi Hills locations (1632 ± 3 Ma; Vallini et al., 2007; Fig. 1). All of these prospects are broadly coeval with the 1650–1600 Ma uranium deposits in the Kombolgie Basin (Fig. 1; Vallini et al., 2007).

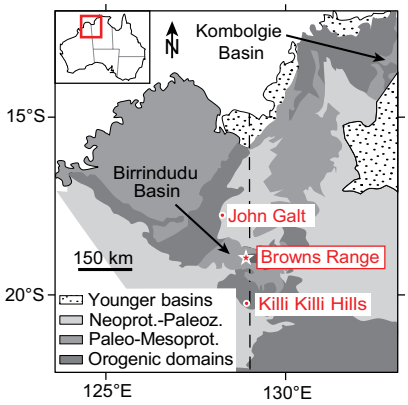

Figure 1. Geological map of Western Australia–Northern Territory border area (after Dunster and Ahmad, 2013), showing Browns Range heavy rare earth element (HREE) deposits, including Wolverine deposit on which present study focuses (star), and related John Galt and Killi Killi Hills occurrences. Mesoprot.—Mesoproterozoic; Neoprot.—Neoproterozoic; Paleoz.—Paleozoic.

Xenotime in the Browns Range has a very uniform chemical composition and is accompanied by hematite and minor light REE (LREE)-bearing florencite–goyazite (Cook et al., 2013). The breccias containing this ore (Fig. 2A) are associated with silicification and smectite–illite replacement of K-feldspar in the surrounding arkoses (Morin-Ka et al., 2016). Nearby granites are 140–180 m.y. older than the xenotime, ruling them out as sources of the REEs (Morin-Ka et al., 2016). In contrast, the regional extent, hydrothermal alteration, and age of the similar xenotime deposits at Killi Killi Hills led Vallini et al. (2007) to speculate on a genetic affiliation with high-grade unconformity-related uranium deposits in other Paleoproterozoic–Mesoproterozoic basins.

SAMPLES AND METHODS

Samples of HREE-mineralized quartz veins and breccia were selected from drill core from the Wolverine deposit. Thin sections of these samples were examined by standard microscopy and cathodoluminescence (CL) imaging. Doubly polished wafers were used to analyze fluid inclusions by

*E-mail: lisa.richter@gmx.net

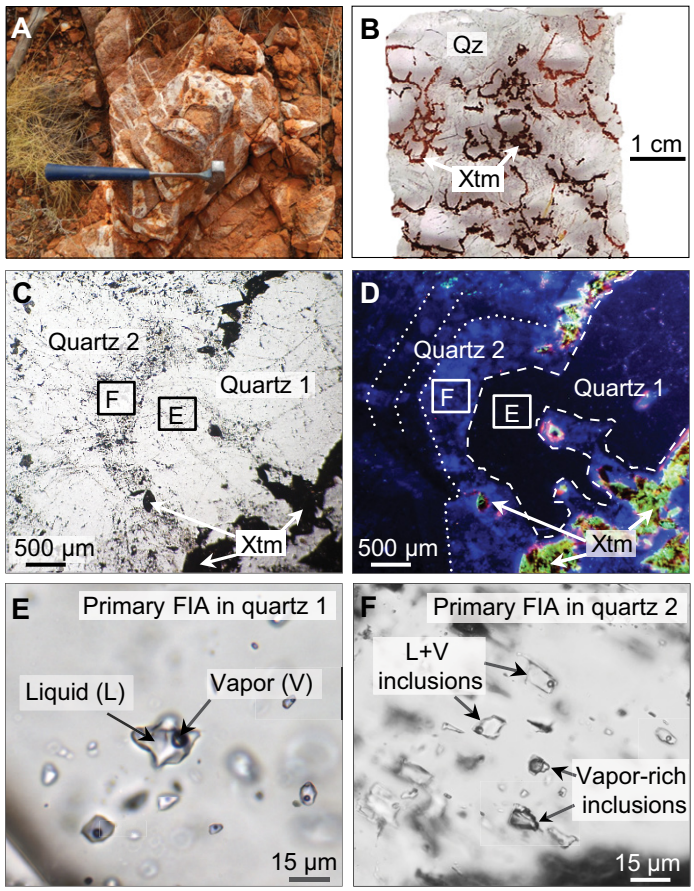

Figure 2. Petrography and paragenesis of quartz-xenotime veins, Wolverine deposit, northern Western Australia (Qz—quartz; Xtm—xenotime; FIA—Fluid Inclusion Assemblage). A: Outcrop of quartz-xenotime vein breccia. B: Brown xenotime mantling brecciated fragments of quartz 1 and intergrown with quartz 2. C: Closeup of sample in B: Quartz 1 with overgrowth of quartz 2, the latter enclosing xenotime inclusions. Also shown are locations of E and F. D: Cathodoluminescence image of area shown in C: Quartz 1 in dark blue, xenotime in yellow-green, and quartz 2 in light blue. E: Quartz 1 enclosing primary assemblage of homogeneously trapped liquid + vapor inclusions. F: Quartz 2 containing primary, heterogeneously trapped liquid + vapor inclusions and vapor-rich inclusions.

microthermometry, Raman spectroscopy, and laser ablation–inductively coupled plasma–mass spectrometry (LA-ICP-MS). Analytical methods and sample locations are detailed in the GSA Data Repository[1].

RESULTS

Petrography and Paragenesis

Xenotime in our samples is present as fine-grained crystals disseminated within the host rock and as coarser-grained, euhedral pyramidal crystals grown into open space, either sitting directly on vein walls or as overgrowths completely mantling the faces of euhedral quartz crystals (Figs. 2B–2D; Fig. DR1 in Data Repository). These overgrowth textures prove in situ precipitation of the xenotime. Four generations of quartz are distinguished by their overgrowth textures, CL colors, and grain sizes. Quartz 1 predates xenotime and shows uniform dark-blue CL (Fig. 2D). Quartz 2 displays growth zonation in tones of light-blue CL (Fig. 2D) and completely encloses inclusions of xenotime arrayed along quartz growth zones, demonstrating that this generation of quartz is cogenetic with xenotime (Figs. 2C and 2D). Quartz 3 overgrows quartz 2 and is characterized by yellow CL (not shown in Fig. 2; see Fig. DR2A). The latest generation, quartz 4, varies from finely crystallized to almost amorphous (Fig. DR2B). Quartz generations 3 and 4 clearly postdate xenotime formation and are not considered further in this study.

Fluid Inclusion Petrography, Microthermometry, and Trapping Conditions

Quartz 1 and quartz 2 contain abundant fluid inclusions displaying clear temporal relationships with respect to xenotime formation. Petrographic features at the scale of individual quartz crystals allow the fluid inclusions to be classified into coeval groups termed "assemblages". Most of the assemblages in quartz 1 occur as three-dimensional clusters of inclusions, showing that they are primary (i.e., of the same age as the host quartz). Each inclusion consists of ~85 vol% aqueous liquid and ~15 vol% aqueous vapor (Fig. 2E; no gases other than H_2O were detected by Raman spectroscopy). This uniformity of phase proportions demonstrates that the inclusions were trapped homogeneously from a single hydrothermal fluid (Diamond, 2003). Microthermometry reveals narrow ranges of ice-melting temperatures, T_m(ice), implying salinities from 0.7 to 1.6 wt% $NaCl_{eq}$ (eq—equivalent), and of temperatures of homogenization (T_h) to the liquid phase from 150 to 170 °C. As the inclusions were trapped homogeneously, these T_h values represent minimum trapping temperatures. Constraints on true trapping temperatures (T_{trap}) are obtained by reconstructing the fluid pressure at the time of entrapment, based on a pressure-temperature (*P-T*) plot of the fluid isochores (Fig. 3). We assume geothermal gradients of 30–40 °C/km and, because the host arkoses are porous and permeable, hydrostatic pressure conditions. Collectively these constraints yield T_{trap} ~170–200 °C at 3.5–6 km depth.

Primary fluid inclusions in quartz 2 are located along crystal growth zones and therefore must have been trapped synchronously with precipitation of quartz 2 and xenotime. The assemblages consist of inclusions with widely varying volume fractions of liquid and vapor. Liquid-rich inclusions contain ≥10 vol% vapor, whereas in end-member vapor-rich inclusions, no liquid is visible (Fig. 2F). The variation in volume fractions of these phases between inclusions in a given assemblage implies that separate liquid and

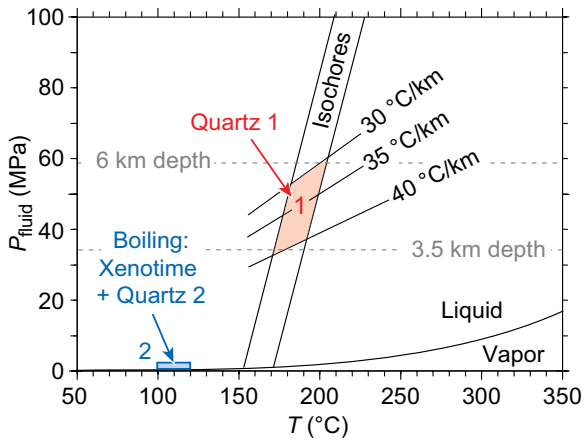

Figure 3. Pressure-temperature (*P-T*) conditions of xenotime precipitation in Wolverine deposit, northern Western Australia. Isochores are for primary, low-salinity, homogeneously trapped fluid inclusions in quartz 1, which predate xenotime mineralization. Area 1 (red)—quartz 1 precipitation at intersection of isochores with feasible hydrostatic gradients; area 2 (blue)—*P-T* of trapping of primary inclusions of vapor + high salinity liquid in quartz 2, which define precipitation conditions of xenotime + quartz 2 + anhydrite + hematite during boiling at low pressure.

[1]GSA Data Repository item 2018074, details of analytical methods, sample locations, microthermometric data, Raman spectra, CL images of quartz generations 3 and 4, and LA-ICP-MS analyses, is available online at http://www.geosociety.org/datarepository/2018/ or on request from editing@geosociety.org.

vapor phases were present during precipitation of quartz 2 and xenotime, i.e., fluid entrapment was heterogeneous (Diamond, 2003). Some of the inclusions contain microscopic crystals of anhydrite (see Fig. DR3 for Raman identification) and hematite. Because the volume fractions of these solids also vary between fluid inclusions within a given assemblage, the same logic as for the liquid and vapor phases applies (Diamond, 2003), i.e., anhydrite and hematite must have been trapped accidentally during fluid entrapment, rather than having precipitated later as daughter phases within the fluid inclusions. This means that both minerals belong to the quartz 2 + xenotime paragenesis. In contrast to hematite, macroscopic anhydrite has not been observed, perhaps due to later dissolution. Temperatures of ice melting show that the aqueous liquid trapped in quartz 2 is of high salinity (23.6–25.8 wt% $NaCl_{eq}$), and the inclusions most rich in liquid homogenize between 100 and 120 °C. As inclusion entrapment occurred from a heterogeneous mixture of liquid and vapor, and as no evidence was found for post-entrapment necking down, the lowest of the T_h values (100 °C) is taken as equivalent to T_{trap}. Similarly, the pressure at homogenization is equivalent to the trapping pressure (P_{trap}). No gases other than H_2O were detected by Raman spectroscopy, therefore P_{trap} is constrained to very low values, barely above 0.1 MPa. The same heterogeneously trapped inclusion assemblages also occur as two-dimensional arrays in healed fractures cross-cutting quartz 1, consistent with them being coeval with quartz 2. See the Data Repository for full analytical results.

Composition of Parent Fluid of Quartz 2 and Xenotime

Metal ratios were determined in individual, primary fluid inclusions by LA-ICP-MS. No meaningful results were obtained on the weakly saline inclusions in quartz 1, but high-quality signals were acquired on the saline inclusions in quartz 2. They reveal that the cations in the fluid that precipitated xenotime were dominated by Na, K, Mg, Ca, and Fe, with detectable contents of Cu, Zn, Y, Pb, U, and REEs. The coprecipitation of anhydrite shows that SO_4^{2-} was present in solution, and the ubiquitous Raman signal of hydrohalite ($NaCl \cdot 2H_2O$; Fig. DR4) below the eutectic temperature of the inclusions shows that the dominant anion was Cl^-. Accordingly, the metal ratios obtained by LA-ICP-MS have been recast into concentrations in the aqueous liquid by combining monovalent KCl with NaCl, and bivalent $MgCl_2$ and $FeCl_2$ with $CaCl_2$, and modelling the measured T_m(ice) values within the ternary H_2O-NaCl-$CaCl_2$ system. Figure 4 compares the resulting mole fractions of metals in the fluid with those in the coexisting xenotime. Making allowances for the Oddo-Harkins effect, the contents of LREEs and HREEs are roughly equal in the fluid, yet the coexisting xenotime is selectively enriched in HREEs (by factors of between 20 for La and 47,000 for Dy) as well as Y (factor of 21,100) and U (factor of 1100). Phosphorus was below detection in the fluid inclusions. The strongly contrasting compositions of the two phases demonstrates that the fluid inclusion analyses are not contaminated by xenotime crystallites. The data in Figure 4 thus represent the effective fractionation of the detected metals between coexisting aqueous solution and xenotime at 100 °C and P_{fluid} = 0.1–0.2 MPa (see Fig. DR6 for partition coefficients). Moreover, the molalities of Y (1.0×10^{-3} mol/kg), REEs (8.5×10^{-6} to 6.7×10^{-5} mol/kg) and U (3.5×10^{-5} mol/kg; right-hand *y*-axis in Fig. 4) correspond to their total solubilities in equilibrium with the xenotime solid solution under these *P-T* conditions.

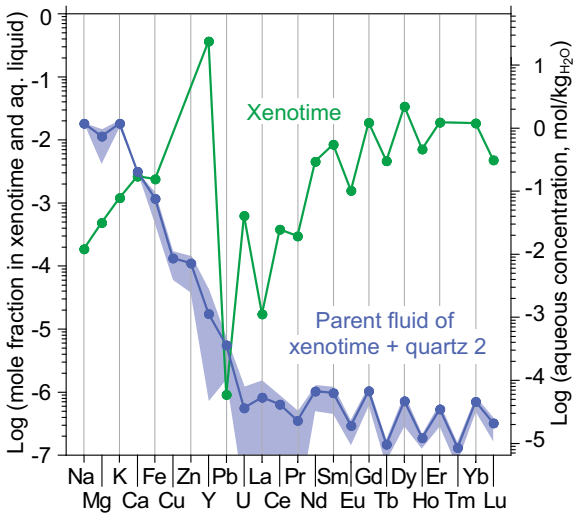

Figure 4. Metal concentrations in xenotime and its coexisting parent hydrothermal fluid, Wolverine deposit, northern Western Australia, determined by laser ablation–inductively coupled plasma–mass spectrometry (LA-ICP-MS). Green curve is average of 86 spot analyses of xenotime (Cook et al., 2013), showing dominance of heavy rare earth elements (HREEs) over light REEs (LREEs) (see scale on left-hand vertical axis). Blue curve and band are analyses of individual primary fluid inclusions in quartz 2 (this study). Blue curve denotes average of three inclusion assemblages, each with 7–9 analyzed inclusions; blue band denotes ±1σ (see alternative scales on left- and right-hand vertical axes). Solid:fluid ratios of metals represent effective fractionation between coexisting phases at 100 °C and P_{fluid} = 0.1–0.2 MPa. aq.—aqueous.

DISCUSSION

Hydrothermal REE Transport

A first issue to discuss is the spectacularly high solubility of the REEs in the parent fluid of xenotime (Fig. 4). The experimentally determined solubility product of end-member xenotime (YPO_4) at 100 °C and 0.1 MPa is extremely low at 10^{-27} (Migdisov et al., 2016). Because the Wolverine xenotime is a REE solid solution, its solubility product will be even lower than that of the end member. Our analyses of 10^{-3} mol/kg Y and 10^{-5}–10^{-6} mol/kg for individual REEs therefore imply vanishingly small concentrations of P in the fluid in the presence of stable aqueous complexes of the metals. Both of the anions detected in the inclusions, Cl^- and SO_4^{2-}, are known to be effective ligands for Y and REEs (Migdisov et al., 2016), and the presence of coeval hematite with xenotime suggests that aqueous sulfur was predominantly in the oxidized state. The first formation constant for the SO_4^{2-} complex is ~$10^{4.6}$ (Migdisov et al., 2016), and although the corresponding value for the Cl^- complex is about three orders of magnitude lower (Migdisov et al., 2016), Cl^- is highly concentrated in the Wolverine fluid. Fluoride is also known to complex REEs exceptionally well at low temperatures (Migdisov et al., 2016), but its concentration in the Wolverine fluid must have been very low, as no fluorite has been found despite aqueous Ca being present in excess. Similarly, OH^- and CO_3^{2-} ligands can be ruled out because the observed sericitization of wall-rock feldspar points to low pH. It is therefore most likely that the high total solubilities of Y and REEs are due to complexing by SO_4^{2-} and Cl^-. Unfortunately, current thermodynamic models do not allow the speciation to be calculated rigorously for this high-salinity fluid in equilibrium with the xenotime solid solution.

Fluid Evolution

The main steps in fluid evolution and formation of the xenotime mineralization can be reconstructed as follows. Quartz 1 precipitated from a hot (~190 °C), low-salinity (0.7–1.6 wt% $NaCl_{eq}$) hydrothermal fluid as it ascended and cooled along fractures or faults leading from the Archean basement into the overlying sediments. We have no information on the nature of the formation waters in the porous arkose wall rocks, although low-salinity, early diagenetic fluids similar to those that precipitated quartz 1 were present at broadly the same time in the Kombolgie Basin (Fig. 1; Kyser and Cuney, 2009). It is therefore not clear if any mixing occurred between the hydrothermal fluid and the adjacent formation water.

Subsequent reactivation of the faults allowed influx of the saline (~25 wt% $NaCl_{eq}$), REE-rich fluid that precipitated quartz 2. The known evaporites in the Birrindudu and Limbunya Groups (Dunster and Ahmad, 2013) could have provided the requisite salinity for this stage 2 fluid. The faulting locally brecciated quartz 1 and created additional space in the veins. We attribute the observed stage 2 fluid boiling to this volume increase, which caused fluid pressure to drop below vapor saturation at 0.1–0.2 MPa. Whereas boiling presumably promoted deposition of the quartz 2 + xenotime + hematite + anhydrite assemblage, the crux of the xenotime precipitation mechanism must lie with the supply of phosphorus. Paired transport of phosphorus and REEs within the stage 2 fluid is ruled out by the low thermodynamic solubility of xenotime, therefore the two components must have first combined via mixing at the site of deposition. The drop in fluid pressure induced by faulting would likely have drained formation water from the porous wall rocks into the vein structures, allowing the stage 2 fluid to boil and mix simultaneously. We assume that this formation water contained the necessary phosphate to form xenotime. Because the stage 2 fluid inclusions in equilibrium with xenotime still contain abundant Y and REEs (Fig. 4), it follows that the amount of xenotime precipitated at the Wolverine deposit was limited by the availability of phosphorus.

Source of REEs

The ultimate source of the REEs in the stage 2 fluid remains unknown. Detrital REE-bearing monazite and apatite in the Paleoproterozoic sediments and underlying Browns Range Metamorphics are possible candidates. Alteration of these minerals or of preexisting U-REE minerals by basinal fluids has been well documented for similar Proterozoic sedimentary basins and their crystalline basement elsewhere (e.g., Kyser and Cuney, 2009).

Link to Unconformity-Related Uranium Deposits

As pointed out by Vallini et al. (2007) for the Killi Killi Hills deposits (Fig. 1), the REE mineralization in the Browns Range shares some key characteristics with unconformity-related, high-grade uranium deposits in the Kombolgie Basin (Fig. 1), including (1) the geotectonic setting, (2) the age of ore formation, (3) the vicinity of faults that traverse the basement-sediment unconformity, and (4) an oxidizing, low-temperature, basinal fluid as metal carrier (Kyser and Cuney, 2009). A further similarity is the elevated concentration of uranium in the stage 2 fluid (3.5×10^{-5} mol/kg; Fig. 4; cf. Richard et al., 2010), despite xenotime itself acting as a sink for U (0.05 mol%; Fig. 4). Thus, with its excess oxidized U, the Wolverine fluid would have been capable of transporting uranium further within the southern Birrindudu sediments and precipitating it where it encountered a suitable reductant, as occurs in unconformity-related uranium deposits (Kyser and Cuney, 2009).

An apparent difference with respect to the uranium deposits is the occurrence of decompression boiling at Wolverine. However, this feature too may turn out to be common to uranium deposits elsewhere. For example, Chi et al. (2017) recently reported fluid boiling in a low-temperature, low-pressure basinal environment at the unconformity-related End uranium deposit, Nunavut, Canada.

CONCLUSIONS

Our fluid inclusion data from quartz coevally precipitated with xenotime provide unique insights into the little-known hydrothermal HREE deposits in sedimentary basins. At the Wolverine deposit, xenotime precipitated along with an oxidized assemblage of hematite and minor anhydrite at 100–120 °C. This demonstrates that significant REE deposition is feasible at normal basin temperatures, and it therefore raises the potential of unconformity settings for REE exploration.

Our data identify SO_4^{2-} and Cl^- as the ligands that enabled REE transport at these low temperatures. Decompression boiling due to faulting-induced volume expansion within the hydrothermal vein system played a key role in xenotime precipitation. Similar sites of tectonic brecciation may therefore be promising exploration targets.

The highly saline ore fluid (~25 wt% $NaCl_{eq}$) was not only boiling during xenotime precipitation, but its excess of REEs in equilibrium with xenotime shows that it must have mixed simultaneously with a second fluid to acquire phosphorus. That the availability of phosphorus limited the amount of xenotime precipitation is demonstrated by the high concentrations of Y (1.0×10^{-3} mol/kg) and individual REEs (8.5×10^{-6} to 6.7×10^{-5} mol/kg) in the fluid in equilibrium with xenotime. The excess metal contents imply that REEs and Y can be effectively transported at typical basin temperatures; the residual fluid at Wolverine is thus still a potent metal carrier.

The observation that the REE-bearing fluid also contains excess U strongly supports the idea, already proposed by others based on geological criteria, that the Browns Range hydrothermal fluid is an analogue of the ore-bearing fluid in world-class unconformity-related uranium deposits found in sedimentary basins of the same age elsewhere.

ACKNOWLEDGMENTS

We thank G. Bauk, R. Wilson, and J. Chapman of Northern Minerals, and S. Rassler for field assistance; J. Götze for CL imaging; and V. Lüders for advice on microthermometry. Helpful comments on the manuscript were provided by J. Brugger, R. Rainbird, A. Richard, and an anonymous reviewer. Banks acknowledges Natural Environment Research Council project SoS RARE (M011429/1).

REFERENCES CITED

Chi, G., Haid, T., Quirt, D., Fayek, M., Blamey, N., and Chu, H., 2017, Petrography, fluid inclusion analysis, and geochronology of the End uranium deposit, Kiggavik, Nunavut, Canada: Mineralium Deposita, v. 52, p. 211–232, https://doi.org/10.1007/s00126-016-0657-9.

Cook, N.J., Ciobanu, C.L., O'Rielly, D., Wilson, R., Das, K., and Wade, B., 2013, Mineral chemistry of Rare Earth Element (REE) mineralization, Browns Range, Western Australia: Lithos, v. 172–173, p. 192–213, https://doi.org/10.1016/j.lithos.2013.04.012.

Diamond, L.W., 2003, Systematics of H_2O inclusions, *in* Samson, I., et al., eds., Fluid Inclusions: Analysis and Interpretation: Mineralogical Association of Canada Short Course 32, p. 55–79.

Dunster, J.N., and Ahmad, M., 2013, Birrindudu Basin, *in* Ahmad, M., and Munson, T.J., compilers, Geology and Mineral Resources of the Northern Territory: Northern Territory (Australia) Geological Survey Special Publication 5, p. 17:1–17:17.

Kyser, K., and Cuney, M., 2009, Recent and not-so-recent developments in uranium deposits and implications for exploration: Mineralogical Association of Canada Short Course 39, 257 p.

Migdisov, A., Williams-Jones, A.E., Brugger, J., and Caporuscio, F.A., 2016, Hydrothermal transport, deposition, and fractionation of the REE: Experimental data and thermodynamic calculations: Chemical Geology, v. 439, p. 13–42, https://doi.org/10.1016/j.chemgeo.2016.06.005.

Morin-Ka, S., Beardsmore, T.J., Hancock, E.A., Rasmussen, B., Dunkley, D., Zi, J., Muhling, J., Wilson, R., and Chapman, J., 2016, Alteration and age of the Browns Range heavy rare earth element deposits, *in* GSWA 2016 Extended Abstracts: Promoting the Prospectivity of Western Australia: Geological Survey of Western Australia Record 2016/2, p. 21–25.

Rabiei, M., Chi, G., Normand, C., Davis, W.J., Fayek, M., and Blamey, N.J.F., 2017, Hydrothermal rare earth element (xenotime) mineralization at Maw Zone, Athabasca Basin, Canada, and its relationship to unconformity-related uranium deposits: Economic Geology and the Bulletin of the Society of Economic Geologists, v. 112, p. 1483–1507, https://doi.org/10.5382/econgeo.2017.4518.

Richard, A., Pettke, T., Cathelineau, M., Boiron, M.-C., Mercadier, J., Cuney, M., and Derome, D., 2010, Brine-rock interaction in the Athabasca basement (McArthur River U deposit, Canada): Consequences for fluid chemistry and uranium uptake: Terra Nova, v. 22, p. 303–308, https://doi.org/10.1111/j.1365-3121.2010.00947.x.

Vallini, D.A., Groves, D.A., McNaughton, N.J., and Fletcher, I.R., 2007, Uraniferous diagenetic xenotime in northern Australia and its relationship to unconformity-associated uranium mineralization: Mineralium Deposita, v. 42, p. 51–64, https://doi.org/10.1007/s00126-005-0012-z.

Manuscript received 18 July 2017
Revised manuscript received 16 December 2017
Manuscript accepted 19 December 2017

Printed in USA